Available online at www.sciencedirect.com
SCIENCE DIRECT®

Journal of Catalysis 223 (2004) 13–27

JOURNAL OF CATALYSIS

www.elsevier.com/locate/jcat

Reduction of N_2O with CO over FeMFI zeolites: influence of the preparation method on the iron species and catalytic behavior

Javier Pérez-Ramírez,[a,*] M. Santhosh Kumar,[b] and Angelika Brückner[b]

[a] *Norsk Hydro, Agri Research Centre, Nitric Acid Technology, PO Box 2560, N-3907, Porsgrunn, Norway*
[b] *Institute for Applied Chemistry Berlin–Adlershof, Richard-Willstätter-Str.12, D-12484, Berlin, Germany*

Received 11 November 2003; revised 6 January 2004; accepted 6 January 2004

Abstract

The reduction of N_2O by CO was investigated over FeMFI zeolites prepared by different methods including sublimation, liquid ion exchange, and hydrothermal synthesis followed by steam activation. This leads to catalysts with different nature and distribution of iron species, as characterized by HRTEM, UV/vis, and EPR techniques. A common denominator in the FeZSM-5 samples is the heterogeneous iron constitution, with a significant degree of clustering in the form of iron oxide particles. Iron clustering was suppressed in steam-activated Fe-silicalite, presenting a remarkable uniform distribution of isolated iron species. In the presence of CO, the conversion of N_2O over the catalysts is strongly accelerated with respect to direct N_2O decomposition. The reaction rate increases linearly with the molar CO/N_2O feed ratio and strongly depends on the preparation method applied. A correlation was found between the fraction of isolated Fe(III) species in the as-prepared catalysts and the activity for N_2O reduction with CO. Steam-activated Fe-silicalite, containing mostly isolated iron ions in extraframework positions, shows the highest activity per mole of iron, while the highly clustered liquid-ion-exchanged catalyst presents the lowest activity. In situ UV/vis and EPR studies evidence the participation of mononuclear iron ions in the N_2O–CO reaction, and also support the involvement of oligonuclear Fe_xO_y species. The reaction mechanism is iron site dependent. Over isolated sites, the reduction of N_2O with CO occurs via coordinated CO species on Fe^{3+} ions. The reaction over oligonuclear sites proceeds via a redox Fe^{3+}/Fe^{2+} process with intermediate formation of O^- radicals.

Keywords: Fe-zeolites; FeMFI; Preparation method; N_2O decomposition; N_2O reduction; CO; Iron species; Active sites; Mechanism; In situ UV/vis; In situ EPR

1. Introduction

Fe-zeolites show a remarkable performance in various N_2O conversions, including its abatement (N_2O decomposition and selective catalytic reduction) as well as its utilization as a selective oxidant [1–3]. Early studies with this catalytic system aimed at elucidating mechanistic and kinetics aspects of the direct N_2O decomposition [4,5]. This reaction is initiated by the activation of N_2O on a vacant site, leading to O^* species [Eq. (1)]. This atomic oxygen species, otherwise referred to as α-oxygen, has unique properties in selective oxidation processes involving hydrocarbons, like the direct hydroxylation of benzene to phenol [3] and the oxidative dehydrogenation of propane to propene [6]. In direct N_2O decomposition over Fe-zeolites, two different mechanisms were postulated for regeneration of the active site [1,4]: the reaction of a second N_2O molecule with the oxidized site [Eq. (2)] and the recombination of adsorbed oxygen atoms [Eq. (3)]. Some of us concluded that O_2 is mainly produced by recombination of atomic oxygen based on TAP (temporal analysis of products) experiments under high vacuum in the temperature range of 573–973 K [7,8], while Nobukawa et al. [9] obtained experimental evidence for Eq. (2) using an ^{18}O-tracer technique at 693 K and atmospheric pressure.

$$N_2O + {}^* \rightarrow N_2 + O^*, \quad (1)$$

$$N_2O + O^* \rightarrow N_2 + O_2 + {}^*, \quad (2)$$

$$2O^* \rightarrow O_2 + 2^*, \quad (3)$$

$$CO + O^* \rightarrow CO_2 + {}^*. \quad (4)$$

Although the mechanism of O_2 formation is not completely resolved, it is widely accepted that oxygen desorption is a rate-determining step during N_2O decomposition

---

[*] Corresponding author.
E-mail address: javier.perez.ramirez@hydro.com (J. Pérez-Ramírez).

0021-9517/$ – see front matter © 2004 Elsevier Inc. All rights reserved.
doi:10.1016/j.jcat.2004.01.007

over Fe-zeolites [7–9]. The presence of reducing agents accelerates the removal of atomic oxygen from the catalyst surface by selective catalytic reduction (SCR), resulting in a decreased operation temperature. This magnitude ranges between 50 and 100 K and depends on the nature of the reductant and its partial feed pressure. The SCR of N_2O over Fe-zeolites has been investigated using various hydrocarbons, ammonia, and carbon monoxide [10–12]. Delahay et al. [11] concluded that CO was the most efficient selective reductant for N_2O over ion-exchanged Fe-BEA at low temperatures in the presence of oxygen, showing significant activities at 470 K. Previously, Kapteijn et al. [12] reported the enhanced N_2O decomposition activity over an ion-exchanged FeZSM-5 in the presence of CO around 673 K. The proposed microkinetic model assumes that CO removes adsorbed atomic oxygen according to an Eley–Rideal mechanism [Eq. (4)]. Following the reaction pathway in Eqs. (1)–(4), in the presence of an efficient oxygen remover like CO, the overall rate of N_2O reduction can approach that of N_2O activation by Eq. (1). Accordingly, CO can probe the reactivity of oxygen species adsorbed on various iron sites of Fe-zeolites, resulting from N_2O activation. Panov and co-workers [13,14] concluded that CO reacts with α-oxygen in a stoichiometric ratio 1:1, further supporting a reduction mechanism via Eq. (4).

To the best of our knowledge, detailed studies of the reaction between N_2O and CO over Fe-zeolites with different forms of iron species have not been reported. The preparation method of iron-zeolites is critical for obtaining catalysts with a desired performance [15–18], and the intrinsic reaction mechanism ultimately determines the optimal structures of the active site [19]. Hence, fundamental knowledge of the N_2O–CO reaction with respect to the active iron site architecture(s) and mechanism will have valuable implications for catalyst design in conversions involving N_2O.

The present work was undertaken to examine the catalytic behavior of differently prepared FeMFI zeolites in the reduction of N_2O by CO. The nature and distribution of iron in the catalysts was determined by HRTEM, UV/vis, and EPR techniques. Steady-state activity tests at different molar CO/N_2O feed ratios in the temperature range of 475–900 K evidenced the influence of the iron constitution in the zeolites on the catalytic performance. The correlation of steady-state activity data with characterization by ex situ techniques and in situ UV/vis and EPR spectroscopies enables insights be gained into the nature of the active species involved in the catalytic process and the associated reaction mechanism.

2. Experimental

2.1. Catalyst preparation

The chemical composition of the zeolites used in this study was determined by ICP and is presented in Table 1.

Table 1
Chemical composition of the catalysts used in this study, as determined by ICP-OES

Catalyst	Method	Si/Al	Si/Fe	Fe (wt%)
ex-Fe-silicalite	Steam activation	∞	150	0.68
ex-FeZSM-5	Steam activation	31	150	0.67
Fe/ZSM-5	Sublimation	14	14	5.0
Fe-ZSM-5	Liquid ion exchange	37	65	1.4

Details on the preparation and characterization of the catalysts can be found elsewhere [8,20,21]. *Ex*-FeZSM-5 and *ex*-Fe-silicalite were prepared by isomorphous substitution of iron in the zeolite framework followed by calcination (at 823 K for 10 h) and steam activation (partial steam pressure of 300 mbar H_2O and 30 ml STP min^{-1} of N_2 flow at 873 K for 5 h). Fe/ZSM-5 was prepared by sublimation of $FeCl_3$ on HZSM-5 (Degussa), according to the method described by Chen and Sachtler [22]. Fe-ZSM-5 was prepared by liquid (aqueous) ion exchanged with diluted solutions (0.30 mM) of $Fe(NO_3)_3 \cdot 9H_2O$. The parent zeolite was provided by Zeolyst (NH_4-ZSM-5; CBV8020). The exchange was carried out at room temperature under vigorous stirring for 15 h, without control of the pH. The ion-exchanged zeolite was then filtered, washed thoroughly, dried, and finally calcined in static air at 823 K for 5 h.

2.2. Catalyst characterization and in situ studies

Transmission electron microscopy (HRTEM) was carried out on a Philips CM 30 T electron microscope with a LaB_6 filament as the source of electrons operated at 300 kV. The zeolites were amorphized by the electron beam in order to enhance the visibility of the small iron oxide particles.

UV/vis-DRS (diffuse reflectance spectroscopy) measurements were performed with a Cary 400 spectrometer (Varian) equipped with a diffuse reflectance accessory (Praying Mantis, Harrick). To reduce light absorption, samples were diluted by α-Al_2O_3 (calcined at 1473 K for 4 h) at a ratio of 1:3. Deconvolution of the UV/vis spectra into subbands was performed applying Gaussian lineshape functions with GRAMS/32 (Galactic), which uses a least-square fitting algorithm. In situ UV/vis measurements were carried out in a heatable reaction chamber equipped with a temperature programmer and a gas-dosing system with mass-flow controllers. The effect of reductive and oxidative treatments over some samples was analyzed by treatment with 200 mbar H_2 in N_2 and air at 773 K and ambient pressure for 1 h, respectively. Afterward, the sample was cooled down to room temperature in the same mixture and the spectrum was then recorded. In situ experiments with N_2O and CO were performed according to the following sequence: (a) pretreatment in air (15 ml min^{-1}) at 773 K for 1 h and cooling down to 623 K (denoted as the reaction temperature), (b) changing the flow from air to 20 mbar N_2O in He (12.5 ml min^{-1}) for 1 h, (c) switching to 20 mbar CO in He (12.5 ml min^{-1})

for 1 h, and finally (d) switching back to 20 mbar N_2O in He (12.5 ml min^{-1}) at the reaction temperature.

EPR spectra in X band ($\nu \approx 9.5$ GHz) were recorded with the cw spectrometer ELEXSYS 500-10/12 (Bruker). Measurements were typically performed at 298 and 77 K and for some samples spectra were recorded after evacuation at 10^{-2} Pa. The magnetic field was measured with respect to the standard 2,2-diphenyl-1-picrylhydrazyl hydrate (DPPH). In situ measurements were carried out in a self-constructed EPR packed-bed reactor [23] using the sequence described for in situ UV/vis experiments. Additional in situ EPR experiments over Fe/ZSM-5 were performed at 623 K and atmospheric pressure with mixtures of 10 mbar $N_2O + 10$ mbar CO in He (25 ml min^{-1}) and 6.6 mbar $N_2O + 13.4$ mbar CO in He (18.7 ml min^{-1}). For on-line analysis of N_2 formed during the N_2O–CO reaction, the outlet of the EPR reactor was connected to a capillary gas chromatograph (Shimadzu GC 17AAF) equipped with a thermal conductivity detector and a Molsieve 5A column.

2.3. Activity tests

Activity measurements were carried out in a parallel-flow reactor system, similar to that described in [24], using 50 mg of catalyst (125–200 µm) and space times of 3×10^5 and 9×10^5 g s mol^{-1} at atmospheric pressure. The space time is defined as the ratio $W/F(N_2O)_o$, where W is the catalyst mass and $F(N_2O)_o$ the molar flow of N_2O at the reactor inlet. The catalyst beds were homogeneously diluted with silicon carbide (125–200 µm) in a volumetric ratio 1:1, in order to improve heat transfer and minimize axial dispersion in the bed. At such a degree of dilution the conversion measured is not affected by the presence of diluent [25]. Feed mixtures containing N_2O (1.5 mbar) and CO (0–1.5 mbar) in He were applied. Before reaction, the catalysts were pretreated in 1.5 mbar N_2O in He at 723 K for 1 h and cooled in that gas flow to the initial reaction temperature. The temperature was increased at intervals of 25 K in the range 475–900 K. This cycle was followed by a stepwise decrease of temperature at 25 K intervals. In this temperature range deactivation of the catalysts was absent and up and down cycles lead to very similar activity curves. Generally, 1 h after a change of conditions (temperature and feed composition), the N_2O conversion levels were constant and considered as the steady state. The product gases were analyzed with a GC (Chrompack CP 9001) equipped with a thermal conductivity detector, using a Poraplot Q column (for CO_2 and N_2O separation) and a Molsieve 5A column (for N_2, O_2, and CO separation). During the experiments, the mass balances of N, C, and O closed at $> 98\%$. N_2O and CO conversions were calculated from the amount of N_2 and CO_2 formed, respectively.

3. Results

3.1. Characterization of iron species

Table 1 shows the chemical composition of the catalysts used in this study. The iron content in the steam-activated catalysts is very similar (~ 0.68 wt% Fe), about three and eight times lower than in the catalysts prepared by ion exchange in aqueous solution (1.4 wt% Fe) and in gas phase (5 wt% Fe), respectively. The Al content in *ex*-Fe-silicalite was below the detection limit of the technique (< 100 ppm).

The morphology of the different catalysts was investigated by HRTEM (Fig. 1). The catalysts prepared by liquid ion exchange and sublimation showed an extensive agglomeration of iron species into large iron oxide particles of a certain size distribution. In general, particles were larger in Fe-ZSM-5 (7–25 nm) despite the lower iron content compared to Fe/ZSM-5, where the particle size distribution is in the range of 3–12 nm. Exceptionally, larger particles were identified in the later sample. Iron clustering in the steam-activated catalysts, with a relatively lower iron content, shows important differences compared to the catalysts prepared by ion-exchange and sublimation methods. The degree of iron clustering in *ex*-FeZSM-5 is significant, but relatively small particles with a homogeneous distribution (1–2 nm) were identified. Remarkably, no iron oxide particles were detected in *ex*-Fe-silicalite, indicating the high iron dispersion in this matrix.

UV/vis-DRS spectroscopy was used to investigate the nature of Fe(III) species in the catalysts. The measured spectra of as-prepared zeolites without any pretreatment were converted into Kubelka–Munk functions and deconvoluted into Gaussian subbands that can be assigned to $Fe^{3+} \leftarrow O$ charge-transfer (CT) bands (Fig. 2). This deconvolution was made based on the below assignments and is quantified in Table 2. It is well known that for Fe^{3+} sites, two CT bands associated to $t_1 \rightarrow t_2$ and $t_1 \rightarrow e$ transitions are expected. For isolated Fe^{3+} species, they fall in the high-energy range of the spectrum [26–28]. Thus, the first maximum of the spectra below 300 nm in Fig. 2 has been deconvoluted into two subbands, which are attributed to the $t_1 \rightarrow t_2$ and $t_1 \rightarrow e$ transitions of isolated Fe^{3+} ions. It is complicated to discern whether the isolated Fe^{3+} species are in tetrahedral or higher coordination. CT bands of tetrahedral iron incorporated in the framework of silicalite have been observed at 215 and 241 nm [26], and a band at 278 nm is observed for isolated Fe^{3+} species in octahedral coordination in Al_2O_3 [27].

Octahedral Fe^{3+} ions in small oligonuclear clusters ($Fe_x^{3+}O_y$) give rise to broad bands between 300 and 450 nm and bands above 450 nm are characteristic for larger Fe_2O_3 particles [26]. To determine the nuclearity and structure of these small oligonuclear iron clusters is a very challenging aspect but is out of the scope of this paper. Analogously to the case of isolated Fe^{3+} ions, $t_1 \rightarrow t_2$ and $t_1 \rightarrow e$ transitions are expected for Fe^{3+} in oligonuclear Fe_xO_y species. Light absorption in the spectra of Fig. 2 above 300 nm occurs in a

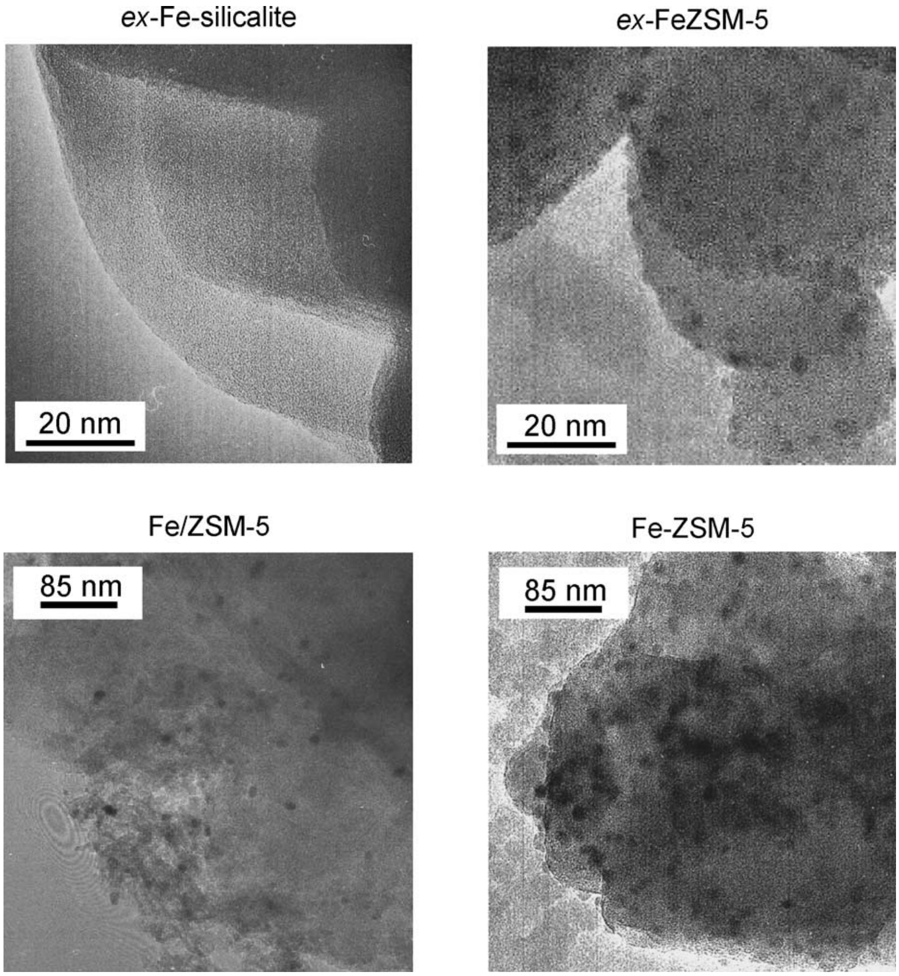

Fig. 1. HRTEM micrographs of the FeMFI zeolites investigated in this study.

Table 2

Percentage of the area of the subbands (I_1 at $\lambda < 280$ nm, I_2 at $280 < \lambda < 400$ nm, and I_3 at $\lambda > 400$ nm) estimated by deconvolution of the UV/vis-DRS spectra (I_{total}) of the catalysts (see Fig. 2) and corresponding Fe percentage derived from total Fe content (see Table 1) (assumptions applied in the fitting procedure are described in the text)

Catalyst	I_1[a] (%)	Fe_1 (wt%)	I_2[b] (%)	Fe_2 (wt%)	I_3[c] (%)	Fe_3 (wt%)	I_{total} (a.u.)
ex-Fe-silicalite	70	0.47	30	0.20	–	–	31.0
ex-FeZSM-5	30	0.21	62	0.41	8	0.05	30.0
Fe/ZSM-5	26	1.30	67	3.40	6	0.30	85.8
Fe-ZSM-5	15	0.21	52	0.75	33	0.47	57.6

[a] Isolated Fe^{3+} ions in tetrahedral and higher coordination.

[b] Oligonuclear $Fe_x^{3+}O_y$ clusters.

[c] Large Fe_2O_3 particles.

very broad range, and therefore certain oligonuclear clusters and larger Fe_2O_3 species may overlap in the deconvoluted bands. Nevertheless, these subbands should be understood in terms of reflecting a semiquantitative distribution of different cluster geometries and sizes rather than representing a certain number of different individual clustered species.

The relative percentage of the different iron species determined in Table 2 does not account for the dependence of the extinction coefficient on the wavelength. Despite this fact and the intrinsic uncertainty of the deconvolution procedure, the quantification in Table 2 provides a valuable indication of the relative amount of various iron site structures among the catalysts investigated. The values in Table 2 do not take into account the contribution of eventual Fe^{2+} species present in the as-prepared samples, although no significant increase of the UV/vis band intensities, due to oxidation of Fe^{2+} to Fe^{3+}, has been observed after air treatment of the catalysts at 773 K (see below and Fig. 3).

In general, $d-d$ transitions of Fe^{3+} are expected between 350 and 550 nm. However, they are symmetry and spin forbidden and, therefore, extremely weak. Moreover, they overlap with the tail of the low-energy CT bands. Hence, interpretation of the spectra is focused on the intense CT bands. The spectrum of *ex*-Fe-silicalite in Fig. 2 and the relative percentage of the deconvoluted subbands in Table 2 indicate that the majority of Fe^{3+} species in the sample is well isolated. The band at ~ 300 nm suggests that a relatively small fraction of iron is present as small oligonuclear species. No contribution > 450 nm was observed, indicating the absence of large Fe_2O_3 particles, in good agreement with HRTEM. In contrast to *ex*-Fe-silicalite, the percentage of

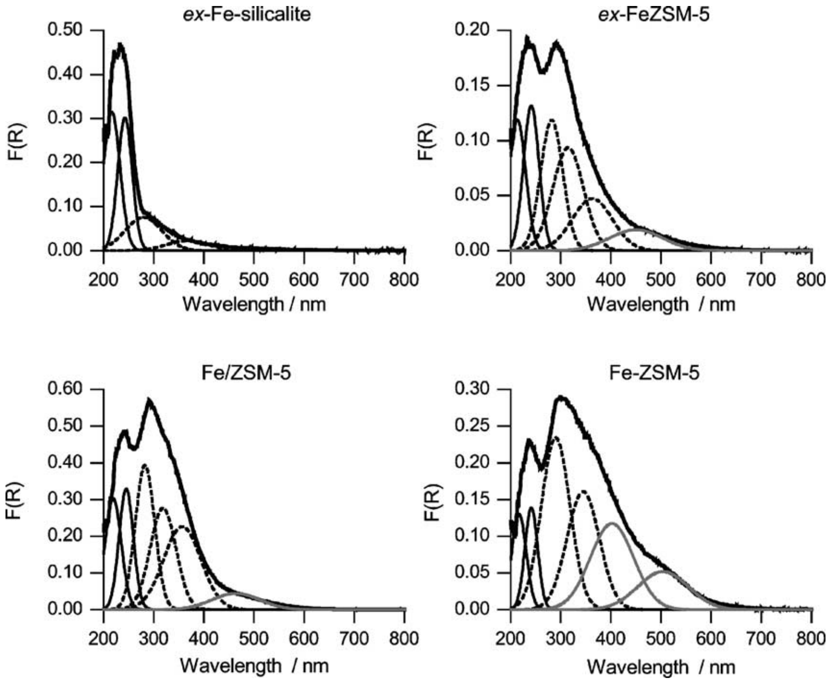

Fig. 2. UV/vis-DRS spectra and deconvoluted subbands of the as-prepared FeMFI zeolites, without pretreatment.

isolated Fe^{3+} species is significantly lower in *ex*-FeZSM-5, with extensive formation of $Fe_x^{3+}O_y$ clusters and a small fraction of Fe_2O_3 particles (Fig. 2 and Table 2). The latter can be attributed to the 1- to 2-nm nanoparticles observed in this sample by electron microscopy (Fig. 1). The fraction of oligonuclear oxo clusters and iron oxide particles in the catalysts prepared by liquid ion exchange and sublimation is even more pronounced. As concluded from the deconvolution in Table 2, Fe-ZSM-5 shows the highest percentage of large Fe_2O_3 particles, which is also in line with HRTEM results.

Heating *ex*-FeZSM-5 in a flow of air for 1 h at 773 K leads to a spectrum with slightly higher intensities (not shown) to of the partial oxidation of Fe^{2+}, present in the original sample, to Fe^{3+}. Divalent iron does not contribute to the UV/vis spectrum, since its bands fall in the near-infrared range around 1000 nm [29]. A certain oxidation of iron(II) was also observed in Fe/ZSM-5 and Fe-ZSM-5 but was hardly visible in Al-free *ex*-Fe-silicalite. In agreement with our results, previous Mössbauer investigations of FeZSM-5 zeolites, prepared by adding Fe to the synthesis gel, have concluded a more favorable formation of Fe^{2+} in matrices with relatively high Al contents [30].

Previous voltammetric characterization has shown that the extraction of framework iron in *ex*-Fe-silicalite is substantial after steam treatment at 873 K, but not complete [21]. As noted previously, the single application of UV/vis does not enable a clear discrimination between isolated Fe^{3+} ions in framework or extraframework positions. However, the influence of Fe^{3+} reduction by H_2 and reoxidation by air on the UV/vis spectrum of the calcined and steamed Fe-silicalite samples can be used to further assess the degree of iron extraction. After hydrothermal synthesis and calcination at 823 K, Fe-silicalite shows typical CT bands at 215 and 241 nm (Fig. 3), originating from iron in the lattice. These bands were not sensitive to a reductive

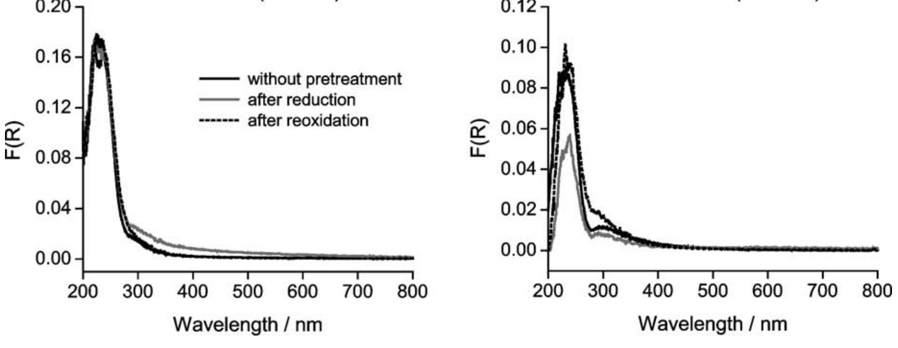

Fig. 3. UV/vis-DRS spectra of the calcined and steamed Fe-silicalite zeolites without pretreatment, after reduction in 200 mbar H_2 in N_2 for 1 h, and after reoxidation in air at 773 K for 1 h.

treatment (200 mbar H_2 in N_2 at 773 K for 1 h). This is expected for isomorphously substituted iron(III) ions, which are well shielded in the zeolite framework, being resistant against reduction. In the calcined sample, a small shoulder at 300 nm was also observed, which indicates that a small fraction of (slightly agglomerated) iron was not incorporated in the framework during the hydrothermal synthesis or, most likely, was already extracted during calcination [20]. Contrarily, the same reductive treatment over steamed *ex*-Fe-silicalite shows that reduction of Fe^{3+} to Fe^{2+} caused a marked decrease of the Fe^{3+} CT band intensity, which is completely reversible on reoxidation in air flow (Fig. 3). This redox behavior can be attributed to isolated iron ions in extraframework positions. Thus, the extraction of iron upon steaming of Fe-silicalite at 873 K is extensive, leading to isolated extraframework Fe(III) species that can be effectively reduced by H_2.

X-band EPR spectra of the catalysts measured at 298 K and 77 K are shown in Fig. 4. All the samples show typical signals at g' values of 2, 4.3, and 6. Spectra simulation has shown that signals at $g' \sim 4.3$ and $g' \sim 6$ arise from Fe^{3+} sites in strong rhombic or axial distortion when the zero-field splitting is large in comparison to the microwave frequency ($g' \sim 4.3$; $D \geqslant h\nu$, $E = \frac{1}{3}D$; $g' \sim 6$; $D \geqslant h\nu$, $E = 0$) [31]. The magnitude of the zero-field splitting is a measure of the distortion of the Fe^{3+} coordination symmetry, but it does not provide information on the number of coordinating ligands. Accordingly, distorted Fe^{3+} sites in various coordinations can contribute to these signals. In zeolites, the line at $g' \sim 4.3$ has been equivocally assigned to Fe^{3+} sites in tetrahedral coordination, either in framework [32–34] or extraframework positions [35–37], while the line at $g' \sim 6$ is frequently assigned to isolated Fe^{3+} species with higher coordination numbers [38,39]. The EPR signal at $g' \sim 2$ has been typically assigned to iron oxide clusters. However, isolated Fe^{3+} ions in positions of high symmetry (zero-field splitting parameters $D,\ E \approx 0$) also contribute to isotropic lines at $g' \sim 2$ [34,40]. Moreover, it has been demonstrated that small changes of D and E in the range between zero and resonance energy induce dramatic changes in the number and position of observable Fe^{3+} signals [34,41].

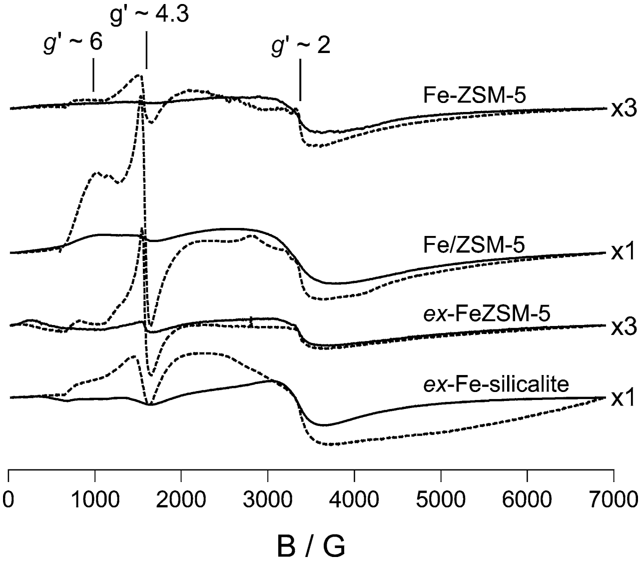

Fig. 4. EPR spectra of FeMFI zeolites (without pretreatment) at room temperature (solid line) and 77 K (dashed line).

The intensity of the line at $g' \sim 2$ in the EPR spectra of the iron zeolites containing clusters (*ex*-FeZSM-5, Fe/ZSM-5, and FeZSM-5) at room temperature and 77 K is very similar (Fig. 4), and does not follow the Curie–Weiss law for paramagnetic species. This suggests that the iron species responsible for this signal are coupled by antiferromagnetic interactions within oxidic clusters, which reduce the number of unpaired spins contributing to the EPR signal. This may explain the fact that the total EPR signal intensity of the clustered zeolites is low as compared to *ex*-Fe-silicalite, since a part of these Fe species is probably EPR silent, as also observed by Kucherov and Shelef [42].

The $g' \sim 2$ signal in *ex*-Fe-silicalite increased upon cooling from room temperature to 77 K, as expected for paramagnetic Fe^{3+} species obeying the Curie–Weiss law. This behavior, generally observed for isolated species, relates to the high degree of dispersion of iron in this catalyst. However, in the EPR spectrum of *ex*-Fe-silicalite at 77 K, a rather narrow line and a very broad line are superimposed in the range of $g' \sim 2$. The latter is not typical for ideally isolated sites without any mutual magnetic interaction and suggests the presence, to some extent, of a weak dipolar interaction between the Fe^{3+} sites contributing to this signal. Therefore, the signal at $g' \sim 2$ in *ex*-Fe-silicalite can be tentatively attributed to highly symmetric and rather isolated Fe^{3+} species, which partly undergo weak dipolar interactions.

Further support for this assignment was gathered by measuring the EPR spectrum of *ex*-Fe-silicalite after evacuation at 10^{-2} Pa and ambient temperature for 2 h. This treatment causes a dramatic decrease of the $g' \sim 2$ line, together with the appearance of additional signals in the low-field range (Fig. 5). This can be attributed to the removal, upon evacuation, of water molecules in the pore network of the zeolite adsorbed on Fe^{3+} species responsible of the EPR signal. This leads to isolated Fe^{3+} sites in a lower symmetry (higher zero-field splitting) that give rise to additional signals in the low-field range. These spectral changes are slowly reversible when exposing the sample to ambient conditions. A very similar behavior for the $g' \sim 2$ signal upon evacuation and rehydration at room temperature was also observed by Berlier et al. [43] on iron silicalite ($Si/Fe = 90$) activated at 773–1073 K in vacuum. These authors attributed the $g' \sim 2$ signal to isolated Fe^{3+} ions, which are solvated by water molecules under ambient conditions. Following this assignment, the result in Fig. 5 further corroborates that the Fe^{3+} species contributing to the $g' \sim 2$ line in *ex*-Fe-silicalite are well isolated in extraframework positions, being accessible to gaseous molecules.

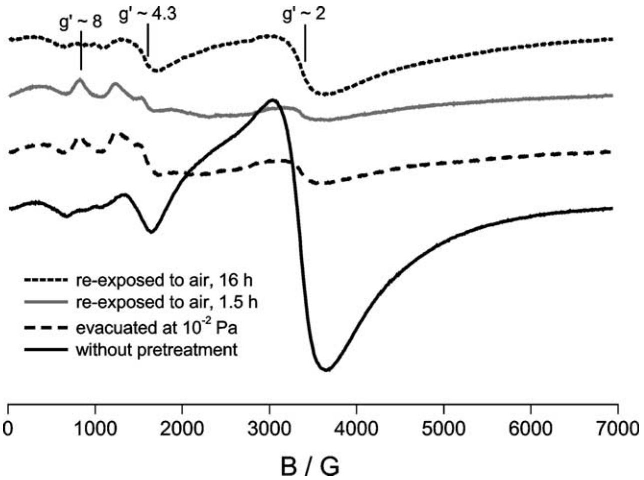

Fig. 5. EPR spectra of *ex*-Fe-silicalite recorded at 298 K before and after evacuation for 2 h and after re-exposure to ambient atmosphere for 1.5 and 16 h.

3.2. Catalytic activity

Fig. 6 shows the N_2O conversion vs temperature resulting from steady-state experiments over *ex*-FeZSM-5 in direct N_2O decomposition and N_2O reduction with CO at two different molar CO/N_2O feed ratios. In the absence of CO, the catalyst shows a significant N_2O conversion above 700 K and a complete conversion at 850 K. Addition of 1.5 mbar CO ($CO/N_2O = 1$) dramatically enhances the N_2O decomposition activity over the catalyst, achieving similar conversions at 100 K lower temperature. The reduction of N_2O by CO also occurs at significantly lower temperatures at a lower partial CO pressure ($CO/N_2O = 0.13$). However, when the limiting reactant CO becomes exhausted (~20% N_2O conversion) the N_2O conversion curve shifts to that of the pure N_2O decomposition. The conversion of CO to CO_2, depicted in Fig. 6, was complete in the range of 700–750 K and is effectively coupled with the conversion of N_2O to N_2. In the experiment with $CO/N_2O = 1$, the amount of CO_2 formed equals the amount of N_2O decomposition (or N_2 formed) at all temperatures, with no formation of O_2, according to Eq. (5). At lower molar CO/N_2O feed ratios ($CO/N_2O = 0.13$), oxygen is produced at high temperatures when CO is consumed and a ratio of $N_2/O_2 = 2$ was obtained, corresponding to the direct decomposition reaction in Eq. (6).

$$N_2O + CO \to N_2 + CO_2, \tag{5}$$

$$N_2O \to N_2 + \tfrac{1}{2}O_2. \tag{6}$$

This general behavior is extrapolable to all the Fe-zeolites investigated in this study. However, the performance strongly depends on each particular sample, which is attributed to the impact of the preparation method on the catalyst constitution with respect to iron. As an example, the N_2O conversion vs temperature over *ex*-FeZSM-5 and Fe/ZSM-5 at four different molar CO/N_2O feed ratios is compared in Fig. 7. The reduction of N_2O with CO is initiated at significantly lower temperatures on the catalyst prepared by sublimation (500 K) as compared to *ex*-FeZSM-5 (> 550 K). Complete N_2O conversion was achieved over Fe/ZSM-5 at 625 K using $CO/N_2O = 1$, while a temperature of 750 K was required over *ex*-FeZSM-5. The shape of the conversion profiles presents important differences too. N_2O conversion over Fe/ZSM-5 increases rapidly in the temperature range of 500–600 K. The reducing agent is consumed at 600 K at $CO/N_2O < 1$ and the N_2O conversion remains practically unchanged until 675 K. The conversion profiles develop more gradually over *ex*-FeZSM-5, not reaching a well-defined plateau at any temperature. The apparent activation energy at $CO/N_2O = 1$ is higher over Fe/ZSM-5 than over *ex*-FeZSM-5 (190 and 128 $kJ\,mol^{-1}$, respectively). These values were estimated around the inflection (50% conversion) of the conversion temperature curves by assuming a plug-flow model and a first-order reaction in N_2O.

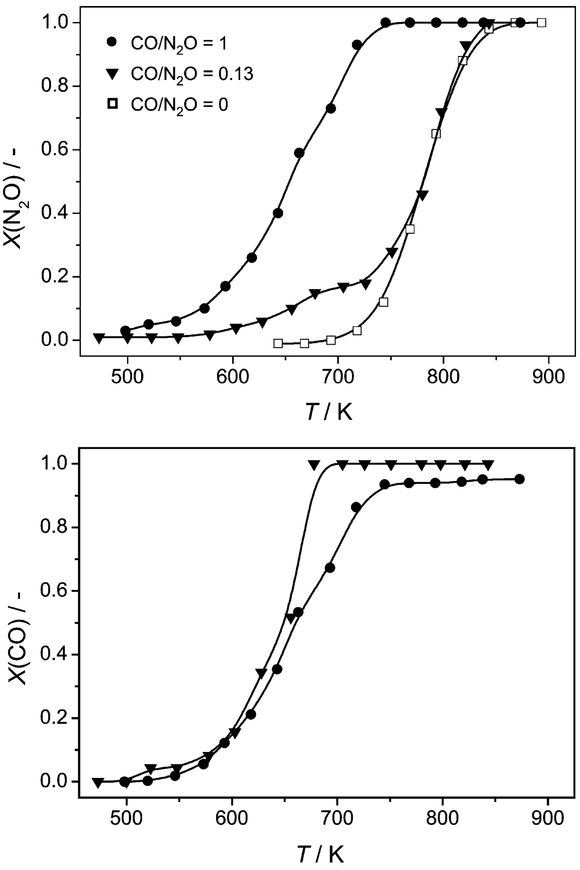

Fig. 6. Conversions of N_2O and CO vs T over *ex*-FeZSM-5 in different feed mixtures at $W/F(N_2O)_0 = 3 \times 10^5$ $g\,s\,mol^{-1}$ and $P = 1$ bar: (□) 1.5 mbar N_2O in He; (▼) 1.5 mbar N_2O and 0.2 mbar CO in He; (●) 1.5 mbar N_2O and 1.5 mbar CO in He.

The N_2O conversion over the catalysts investigated increases linearly with the molar CO/N_2O ratio, as shown in Fig. 8 at 600 K. This temperature was chosen to ensure the presence of CO. At high temperatures CO becomes exhausted over some catalysts, and such comparison would not be representative. The different slope of the fitted lines

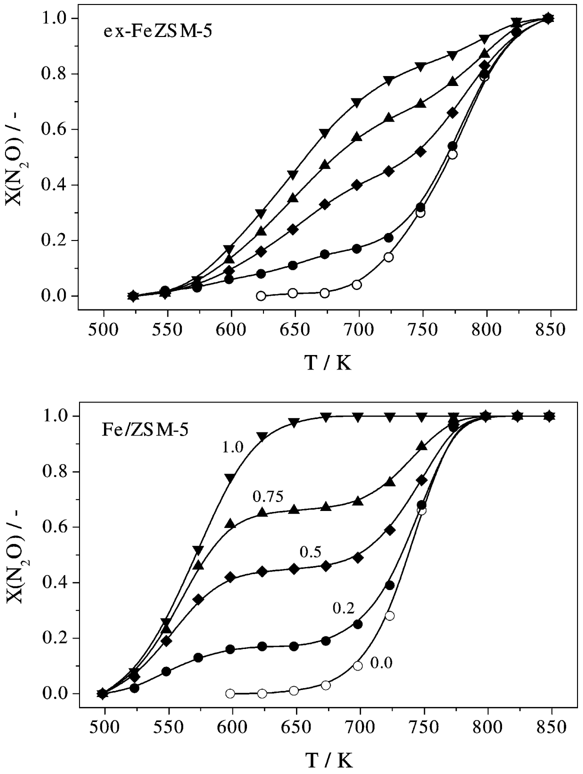

Fig. 7. N_2O conversion vs T over *ex*-FeZSM-5 and Fe/ZSM-5 at different molar CO/N_2O feed ratios (in figure) at $W/F(N_2O)_o = 9 \times 10^5$ g s mol^{-1} and $P = 1$ bar. Partial N_2O pressure was fixed at 1.5 mbar and partial CO pressure was varied from 0 to 1.5 mbar; balance He.

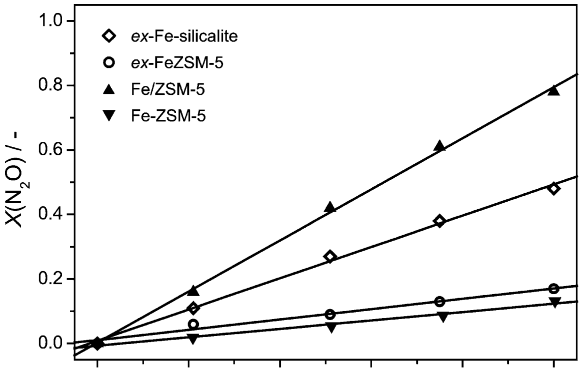

Fig. 8. N_2O conversion at 600 K vs molar CO/N_2O feed ratio over FeMFI catalysts at $W/F(N_2O)_o = 9 \times 10^5$ g s mol^{-1} and $P = 1$ bar. Feed composition as in caption of Fig. 7.

suggests a different kinetic behavior. Fe/ZSM-5 shows the highest N_2O conversions, followed by *ex*-Fe-silicalite. The activity of *ex*-FeZSM-5 and FeZSM-5 is significantly lower. The iron content in Fe/ZSM-5 is ~7 times higher than in *ex*-Fe-silicalite. Accordingly, the later catalyst is clearly superior if the activity is expressed per mole of iron in the sample (about 3 times), indicating a better iron utilization. Since *ex*-Fe-silicalite mainly contains isolated iron ions, it can be assumed that they are responsible for the observed performance. This is supported by comparison with the clustered *ex*-FeZSM-5, prepared using identical methods and with the same iron content, which shows a much lower activity. The high activity of Fe/ZSM-5 should not be connected with the presence of iron clusters, since the relative fraction of isolated iron species, taking into account the iron content and the deconvolution in Table 2, is larger than over *ex*-Fe-silicalite in the test shown in Fig. 8. From our steady-state data and characterization results, a correlation between the fraction of isolated iron sites in the zeolites and the catalytic activity can be qualitatively derived. This correlation is further discussed in Section 4.2. In situ spectroscopic investigations are necessary to confirm the essential role of isolated species and to evaluate the eventual participation of other iron species in the catalytic reduction of N_2O by CO.

3.3. *In situ UV/vis and EPR spectroscopies*

In situ UV/vis and EPR studies were aimed at the identification of active iron species in the reduction of N_2O with CO over FeMFI zeolites, based on the propensity of the iron sites to undergo redox processes. To this end, the interaction of CO, N_2O, and CO + N_2O mixtures with the iron species in the catalysts has been investigated at 623 K. At this temperature, all catalysts have shown substantial activity in steady-state experiments (Section 3.2).

3.3.1. *Steam-activated ex-Fe-silicalite*

Fig. 9 shows that Fe^{3+} species in *ex*-Fe-silicalite are not sensitive to reduction by CO at this temperature, as concluded from the comparison of the UV/vis spectra of the sample in air and in a CO-containing mixture. The EPR spectrum of *ex*-Fe-silicalite changes significantly upon interaction with CO (Fig. 10). The signals at $g' \sim 7.15$, 6.05, and 2, representative for differently distorted isolated sites, decrease in the presence of CO and a new broad signal at $g' \sim 3.01$ appears. The signal at $g' \sim 4.3$ in Fig. 4 is not observed at 623 K, probably due to short relaxation times at high temperatures. Considering the UV/vis results, the decrease of the EPR lines at g' of 7.15, 6.05, and 2 should not be due to reduction of Fe^{3+}. It is plausible to state that CO is chemisorbed on extraframework Fe^{3+} isolated ions, causing changes of the local symmetry and thus altering the position of the EPR signals. A similar shift of the Fe^{3+} signal upon changing ligands was observed for FeZSM-5 zeolites prepared by impregnation of HZSM-5 with a $FeCl_3$ solution [42]. In the as-prepared zeolites, a line at $g' \sim 3.65$ was assigned to isolated $(FeCl_2)^+$ species. Upon calcination in air, this line disappeared due to the transformation of $(FeCl_2)^+$ into differently distorted FeO^+ species, giving rise to EPR signals at $g' \sim 6.5$, 5.6, and 4.27. For *ex*-Fe-silicalite, the EPR changes are reversible upon switching from CO to N_2O (compare Figs. 10a–c). The intensity of the band at 240 nm in the UV/vis spectrum of *ex*-Fe-silicalite is slightly

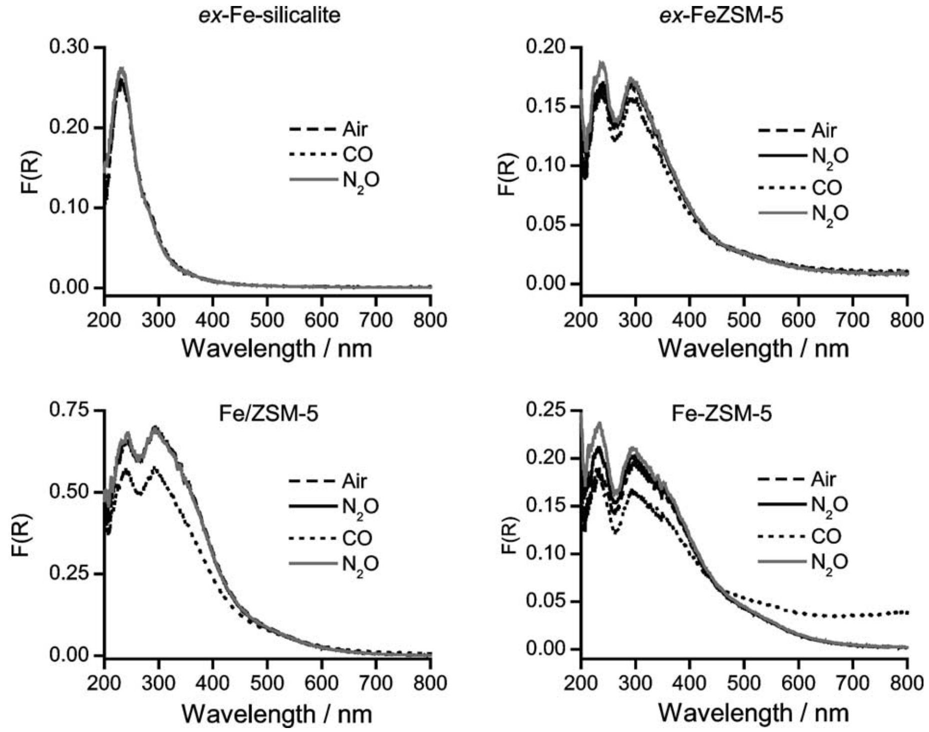

Fig. 9. In situ UV/vis-DRS spectra of FeMFI zeolites at 623 K in different gas mixtures: air, 20 mbar N_2O in He, 20 mbar CO in He, and back to 20 mbar N_2O in He. Spectra were measured after treatment of the samples in the respective mixtures at 623 K for 1 h. Catalyst pretreatment in air at 773 K for 1 h.

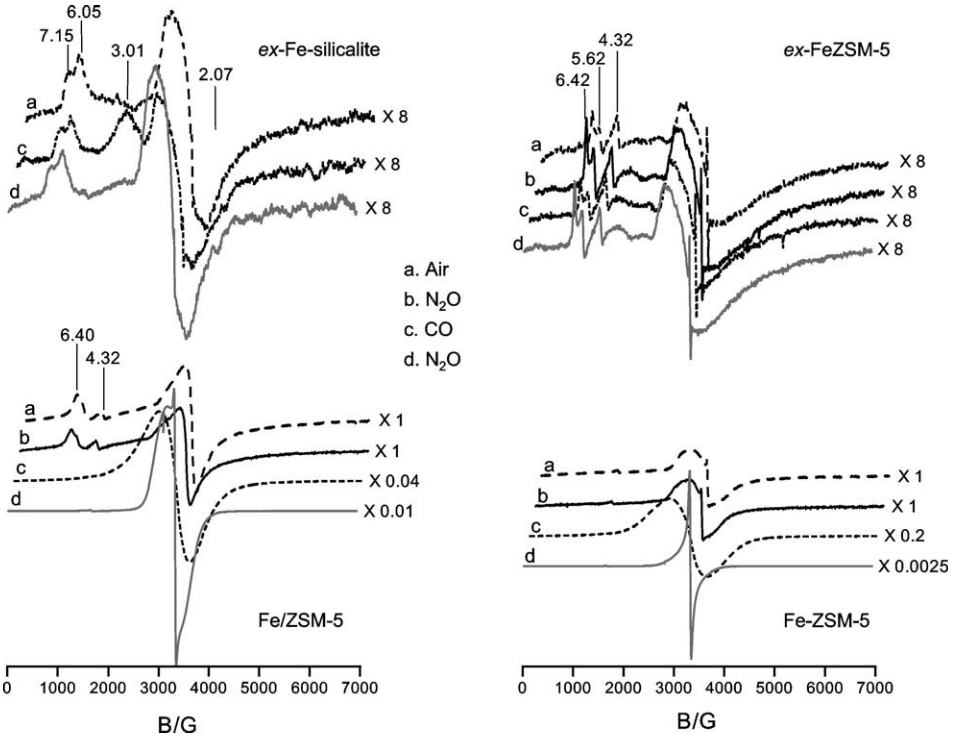

Fig. 10. In situ EPR spectra of FeMFI zeolites at 623 K in different gas mixtures. Conditions as in caption of Fig. 9.

higher after contact with N_2O, as compared to the initial spectrum of the sample in air (Fig. 9). This suggests the presence of small amounts of Fe^{2+} ions in the non-pretreated zeolite, which can be oxidized by N_2O but not by O_2.

3.3.2. *Steam-activated ex-FeZSM-5*

The interaction of CO and N_2O over *ex*-FeZSM-5 leads to important differences compared to *ex*-Fe-silicalite, which are associated with the distinct iron constitution. The UV/vis spectrum of *ex*-FeZSM-5 did not change upon switching from air to N_2O/He, but treatment in CO/He decreases the intensity of the band above 300 nm (Fig. 9), assigned to oligonuclear clusters. Similar to *ex*-Fe-silicalite, the band at 250 nm, characteristic of isolated Fe^{3+} species, remains unaltered. This result suggests a different behavior of Fe^{3+} species upon internation with carbon monoxide: CO reduces oligonuclear $Fe_x^{3+}O_y$ clusters at typical reaction temperatures, while isolated Fe^{3+} ions are more stable against CO reduction. Switching back from CO to N_2O restores the band above 300 nm in *ex*-FeZSM-5 and surprisingly, enhances the band at 250 nm above the maximum reached during the first N_2O treatment. This result can be tentatively explained by assuming that the coordination of some of the Fe^{3+} species reoxidized by N_2O is different from their initial state before reduction with CO. Phenomena like the partial dissolution of larger clusters and/or symmetry changes might lead to an increased absorbance at 250 nm. However, in any case, the changes are very small and the amount of Fe species involved in these processes is not significant.

In the corresponding EPR spectra of *ex*-FeZSM-5 (Fig. 10), switching from air to N_2O causes a slight increase of the signals at $g' \sim 6.42$, 5.62, and 2.0. This can be associated with the change from a mixture containing a paramagnetic gas (O_2) to a diamagnetic one (N_2O), which causes line harrowing since the magnetic interaction between Fe^{3+} and O_2 is suppressed. Interestingly, the signal at $g' \sim 4.32$ is almost not influenced by this change, suggesting that the Fe^{3+} species contributing to this line are not accessible by gas-phase components. Alternatively, it cannot be excluded that traces of iron(II) sites remain in such state after pretreatment in air, but can be oxidized by N_2O.

The signals at $g' \sim 6.42$, 5.62, and 2.0 in *ex*-FeZSM-5 decrease upon switching from N_2O to CO (Fig. 10). Based on the various characterizations in Section 2.1 (HRTEM, UV/vis, and the temperature dependence in the EPR spectra), the signal at $g' \sim 2$ in this sample is assigned to oxidic iron clusters. Accordingly, its decrease upon CO treatment is associated to the reduction of clustered Fe^{3+} species. As observed in *ex*-Fe-silicalite, the decrease of the EPR signals at $g' \sim 6.43$ and 5.62 in *ex*-FeZSM-5 corresponds to isolated Fe^{3+} species, which suffer a change of symmetry upon coordination by CO, but it is not accompanied by their reduction, as concluded from in situ UV/vis. Different than *ex*-Fe-silicalite, no pronounced signal at $g' \sim 3$ was observed in *ex*-FeZSM-5 upon interaction with CO. Furthermore, EPR signals in the low-field range appear at slightly different g-values in the steam-activated Fe-zeolites, suggesting that the distortion of the local symmetry of the isolated sites is unequal in the two catalysts. Coordination of CO in such sites can lead to complexes of slightly different geometry in both samples, causing a shift of the EPR signal. This could also explain the absence of the $g' \sim 3$ signal in *ex*-FeZSM-5. Finally, the EPR signals at $g' \sim 6.42$, 5.62, and 2 were restored upon switching from CO to N_2O (Fig. 10).

3.3.3. *Sublimed Fe/ZSM-5*

As shown in Fig. 9, the UV/vis spectra of Fe/ZSM-5 in air and N_2O were identical. Upon CO treatment, the intensity of the whole spectrum was substantially reduced and completely recovered by switching back to N_2O. The intensity reduction in CO was expected for the bands above 300 nm, arising from clustered iron species. However, the decrease of the band around 250 nm (isolated Fe^{3+} species) was not anticipated, since these species were not reduced by CO in *ex*-Fe-silicalite and *ex*-FeZSM-5. It should be noted that the tail of the CT subbands arising from $Fe_x^{3+}O_y$ clusters in Fe/ZSM-5 extends into the low-wavelength range (see Fig. 2), contributing to the overall intensity below 300 nm. Thus, the marked reduction of the band above 300 nm influences the intensity of the signal at lower wavenumbers.

The EPR spectra of Fe/ZSM-5 show a slight decrease of the signal at $g' \sim 2$ upon switching from air to N_2O, while the signals of isolated Fe^{3+} sites at low field remain practically unchanged (Fig. 10). Subsequent admission of CO leads to a very large broad singlet at $g' \sim 2.07$ in the sample, which is typical of ferrimagnetic Fe_3O_4-like species, and the low-field signals for isolated Fe^{3+} species disappear. This agrees well with previous observations by Kucherov and Shelef [42], who found that even a mild reductive treatment of Fe/HZSM-5 (1 vol% H_2 in He at 573 K) leads to (partial) irreversible loss of isolated Fe^{3+} sites accompanied by the formation of ferrimagnetic Fe_3O_4 clusters. As shown in Fig. 10, switching back from CO to N_2O narrows the line associated with such species. Since the reduced Fe^{2+} sites are totally reoxidized by N_2O, as concluded from UV/vis, the EPR observation should be related to changes of the intrinsic magnetic interactions within the ferrimagnetic clusters. The spectra c and d of Fe/ZSM-5 in Fig. 10 were reproduced upon various periodical treatments in N_2O/He and CO/He mixtures. In N_2O, a very narrow signal at $g' \sim 2.003$ is observed too. Such signal is typical for radical species rather than for Fe^{3+} ions. Panov [3] attributed the unique performance of iron-containing ZSM-5 in the N_2O-mediated oxidation of benzene to phenol to the formation of α-oxygen, whose charge has been a matter of discussion. The ability of N_2O to deposit paramagnetic O^- species on partially reduced oxide surfaces is well known [44]. Such species originate narrow EPR signals near the free-electron g value, having an anisotropic g tensor with $g_\perp > g_\parallel$ [44,45]. However, when they become mobile, e.g., at high temperatures, g anisotropy averages out [45]. To the best of our knowledge, neutral oxygen atoms have never been detected by EPR, due to the short lifetime imposed by the their high reactivity [46]. In a recent work, Starokon et al. [47] concluded that α-oxygen is an anion-radical species, designated as $O_\alpha{}^-$. It has also been shown that O^- species, when engaged in the micropores of CaO/Al_2O_3 crystals with a zeolite-like structure, can be rather stable [45]. Based just on the g value, the narrow isotropic line in Fig. 10 cannot be conclusively assigned to O^- species, since different radical species lead to similar signals in this region. However, considering that the signal appears only in the presence of N_2O and/or after partial reduction of the sample with CO, i.e., under favorable conditions for formation of O^- species, it does not seem unlikely that the signal arises from these radical species, being mobile within the zeolite pore network.

3.3.4. *Ion-exchanged Fe-ZSM-5*

The in situ UV/vis spectra of Fe-ZSM-5 in the low wavelength range are similar to that of Fe/ZSM-5 (Fig. 9). The most significant difference was observed in the visible range upon interaction with CO, leading to an increase of light absorption above 450 nm in the ion-exchanged catalyst. This observation is associated to the lower wavelength tail of an intervalence charge transfer (IVCT) transition, which typically occurs in the near-IR region and is induced by electron delocalization between Fe^{2+} and Fe^{3+} ions. Such a phenomenon is characteristic for mixed-valence iron oxides and has been observed in Fe_3O_4 nanoparticles [48], where the tail of the ICVT transition extends to the visible range and contributes to light absorption above 450 nm. Thus, it is very likely that a similar type of mixed-valence iron oxide particles is formed upon interaction of CO with Fe-ZSM-5. This was not observed over Fe/ZSM-5, with a negligible increase of intensity above 600 nm (Fig. 9). This could be attributed to the significantly larger Fe_2O_3 particles in Fe-ZSM-5, which can more easily undergo reduction to a defined Fe_3O_4-like phase. Furthermore, the mutual distribution of Fe^{3+} and Fe^{2+} species in Fe/ZSM-5 and Fe-ZSM-5 may differ depending on the exact position, intensity, and/or line width of the IVCT transition.

In the EPR spectra of Fe-ZSM-5, signals for isolated Fe^{3+} species are hardly visible, in agreement with the high degree of clustering evidenced by this sample. Large iron oxide particles give rise to the broad EPR signal at $g' \sim 2$ which does not change upon switching from air to N_2O. In the presence of CO, the broad line accounting for ferrimagnetic Fe_3O_4-like particles develops. A similar EPR signal was observed in Fe/ZSM-5 (Fig. 10). However, in the latter sample, the intensity of this line is five times higher than in Fe-ZSM-5, although the total Fe content is only 3.5 times higher (see Table 1). This is likely due to differences in the microstructural domain of the ferrimagnetic particles and not to a higher degree of Fe^{3+} reduction by CO in Fe/ZSM-5, since UV/vis clearly shows a more pronounced reduction in Fe-ZSM-5 (Fig. 9). Upon contact with N_2O, a narrow EPR signal around $g' \sim 2.003$ arises in Fe-ZSM-5. This signal, attributed to O^- species, is 17 times larger than in Fe/ZSM-5, despite the lower iron content in the liquid-ion exchanged sample. These various observations further evidence the markedly different nature of this Fe-oxide phase in both catalysts.

Finally, an in situ EPR experiment was performed by exposing Fe/ZSM-5 to different N_2O–CO mixtures at 623 K (Fig. 11). A change from air to a reaction mixture containing $CO/N_2O = 1$ causes a slight decrease of the signals at $g' \sim 6$ and $g' \sim 2$, while the line at $g' \sim 4.3$ remains unchanged. The N_2O conversion in the experiment was 82%, in good agreement with the steady-state tests in Fig. 7. This result indicates that in the presence of equimolar amounts of N_2O and CO, the average valence of active Fe species is +3 under steady-state conditions, with no formation of ferrimagnetic Fe_3O_4-like particles. This occurs when CO is added in excess ($CO/N_2O = 2$), while the obtained N_2O conversion is slightly increased to 87%.

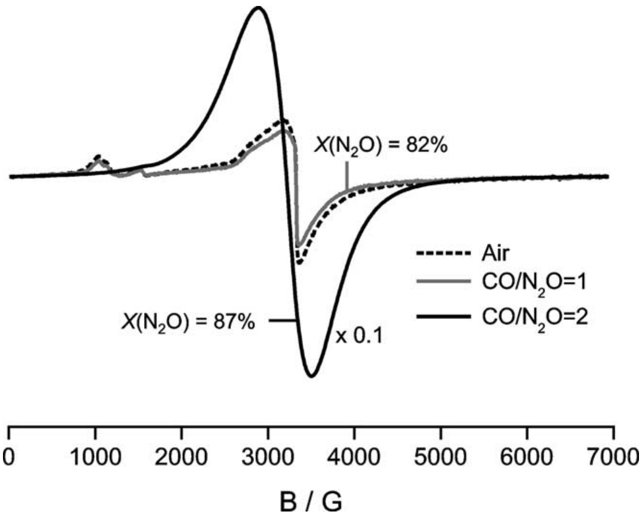

Fig. 11. In situ EPR spectra of Fe/ZSM-5 in different gas mixtures: air at 773 K, 10 mbar N_2O + 10 mbar CO in He ($CO/N_2O = 1$) at 623 K, and 6.6 mbar N_2O + 13.4 mbar CO in He ($CO/N_2O = 2$) at $T = 623$ K and $P = 1$ bar. The N_2O conversion obtained is shown in the figure.

4. Discussion

4.1. *Nature and distribution of iron species*

In this study, FeMFI catalysts were prepared following two general preparation strategies to disperse iron species inside the zeolite channels and cavities: (i) postsynthesis insertion via ion exchange in solution and in the gas phase and (ii) migration of iron to extraframework positions starting from MFI containing isomorphously substituted Fe^{3+}. Postsynthesis methods often lead to intrinsic difficulty of the achievement of a proper cation exchange and highly heterogeneous systems are obtained. The extraction of iron from FeMFI samples exhibiting a unique tetrahedral and isolated iron species is claimed to represent a simpler and more reproducible way to disperse iron species into microporous matrices, although not allowing the insertion of a high percentage of iron [49].

The characterization from the different methods applied (HRTEM, UV/vis, and EPR) to assess the form(s) of iron in the catalysts is in very good agreement. Our results clearly show that the distribution of iron species, as isolated ions, oligonuclear iron species, and iron oxide particles is a function of the sample genesis. A common denominator of the Al-containing Fe-zeolites is the heterogeneous constitution with respect to iron and the extensive degree of clustering. The formation of iron oxide particles at the external surface of the zeolite crystals and their size are more pronounced in the samples prepared by postsynthesis ion exchange methods, especially in the liquid phase. The large particles in Fe-ZSM-5 (up to 30 nm) originate from two processes: precipitation and clustering. In the method applied here, the ion-exchange procedure was performed without pH control, in order to further promote formation of iron oxide particles in the final catalyst. The poor catalytic performance and low redox activity of this sample is in line with the major occurrence of iron in such an inactive form. The liquid ion exchange applied here, to a large extent, mimics the result obtained with a wet impregnation method. Although an improved control of the preparation conditions during liquid ion exchange can lead to a more homogeneous iron distribution in the zeolite, a lack of reproducibility of exchange methods in solution has been frequently reported [16,50–53]. The use of reducing agents and complexing ligands was applied to prevent the precipitation of iron hydroxides and the formation of Brønsted acid sites during synthesis of overexchanged FeZSM-5 ($Fe/Al > 0.5$), but these attempts proved unsuccessful [50].

Ion exchange in the gas phase (sublimation) is undoubtedly a more effective postsynthesis method, since iron clustering is largely suppressed compared to methods in the liquid phase. Sublimation of $FeCl_3$ in the channels of H-ZSM-5 enables a high iron loading in the catalyst ($Fe/Al = 1$). A complete insertion of iron at ion-exchanged positions has been claimed, forming diferric (hydr)oxo-bridge binuclear clusters [22,54,55]. The UV/vis spectrum of Fe/ZSM-5 indeed shows the largest contribution of Fe(III) species in the region of the small oligonuclear iron species in the zeolite channels. However, a uniform distribution of iron species was certainly not achieved in our Fe/ZSM-5, prepared according to the method in [22]. Isolated iron ions and large iron oxide particles (up to 15 nm) are also identified in this sample. The hydrolysis and calcination posttreatments following the sublimation of $FeCl_3$ have proven to be key steps in order to prevent formation of large hematite particles [54,55].

Steam activated *ex*-FeZSM-5 and *ex*-Fe-silicalite are highly diluted samples, with $Si/Fe \sim 150$. The migration of iron from framework to partial or total extraframework positions upon steaming is complex and can be envisaged as a clustering process [21]. An appropriate comparison of the iron constitution in these two samples can be established, since the preparation and activation procedures as well as the iron content in both catalysts were identical. The results obtained over *ex*-FeZSM-5 show that a variety of iron species originated upon steaming, and even the formation of small iron oxide nanoparticles (1–2 nm). Hence a remarkable uniformity of iron species and the absence of extensive clustering are a priori not guaranteed by this method. Of course, the size of the particles is significantly smaller than in the iron-zeolites prepared by postsynthesis methods, which indicates a higher iron dispersion. However, this is also associated to the lower iron content in the sample (e.g., ~ 7 times lower than in the catalyst prepared by sublimation).

A better-defined distribution of iron species was attained upon steam treatment of Fe-silicalite. The color of this sample was nearly white, suggesting the more isolated nature of the iron species in the catalyst, while *ex*-FeZSM-5 was light brownish. Indeed, the majority of iron in *ex*-Fe-silicalite was found as isolated Fe(III) ions in extraframework positions. A very minor degree of iron aggregation is present, as concluded from UV/vis analysis. EPR spectroscopy evidences the paramagnetic behavior of Fe^{3+} species following the Curie–Weiss law, as typically observed for highly symmetric isolated species. However, a certain degree of weak dipolar interactions between Fe^{3+} sites is also identified, indicative of a certain iron association. The amount of iron in the form of aggregates is minimal and of very small size, since they were not detected by HRTEM. Accordingly, the framework composition of the zeolite plays an essential role in determining the iron speciation. In particular, the presence of Al in the MFI structure destabilizes framework iron, promoting extraction and clustering of extraframework species [19,21,30]. Berlier et al. [56] recently concluded, based on infrared studies, that Al favors the dispersion of extraframework iron species in isomorphously substituted FeZSM-5 as compared to Fe-silicalite. In that study, both zeolites were pretreated in vacuum at the same temperature (773 or 973 K). It is well known that the higher stability of iron in the framework of Al-free ferrisilicate requires more severe conditions for extensive extraction of framework iron [21], and thus the term “dispersion” in [56] can be conceptually understood by “degree of iron extraction,” which is obviously associated to reactivity. The results presented here and elsewhere [21], using steam as activation atmosphere (more effective for iron dislodgment that vacuum treatment), show that the higher stability of iron in the framework of silicalite enables a better control of iron extraction upon steam activation, since clustering can be largely prevented. Still, by a proper selection of the steaming temperature (873 K), a substantial degree of Fe extraction can be accomplished, although not being complete. This has been demonstrated by the different reduction characteristics of framework and extraframework isolated iron species during in situ UV/vis in H_2 at 773 K, and previously by voltammetric response studies [21]. Furthermore, the extensive iron dislodgment is expected in view of the high activity of *ex*-Fe-silicalite in the reduction of N_2O with CO (Section 4.2). Framework iron ions are catalytically inactive, since activation of N_2O requires coordination of atomic oxygen to the active site, impossible for framework iron being saturated by surrounding oxygen atoms of the lattice [57,58].

A slight increase of the Fe^{3+} signal appears in the in situ UV/vis spectra of the Al-containing zeolites during O_2 treatment at 600 K, indicating a certain amount of Fe^{2+} in the fresh catalyst, while hardly any oxidation of ferrous ions was observed in *ex*-Fe-silicalite upon oxidative treatment in O_2 or N_2O. Recent XANES work has shown the reduction of Fe^{3+} to Fe^{2+} in Fe-silicalite (in the form of isolated, clustered, or grafted species) upon dislodgment to extraframework positions by thermal treatment in vacuum or in steam [43,49,59]. These extraframework Fe^{2+} species have been characterized by a very high coordinative unsaturation, being able to form $Fe^{2+}(NO)_3$ complexes upon interaction with NO at room temperature [60]. According to Dubkov et al. [61], the reduction of Fe^{3+} to Fe^{2+} upon steam treatment of FeZSM-5 followed by Mössbauer spectroscopy may comprise more than 60% of the total metal content. These Fe^{2+} species, which can be oxidized by N_2O but not by O_2, have been associated with binuclear iron complexes. Our characterization results with *ex*-Fe-silicalite in Sections 3.1 and 3.3 clearly show the practically sole presence of Fe^{3+}, mainly in extraframework isolated positions. FTIR studies of NO adsorbed over *ex*-FeZSM-5 and *ex*-Fe-silicalite at 423–573 K have indeed shown absorption bands of Fe^{2+}–NO, but characteristic bands indicative of more than one nitro group on such iron sites were not identified [62].

4.2. Activity and mechanism of N_2O reduction with CO

In direct N_2O decomposition, O_2 desorption is a rate-determining step, which can be accelerated at a high temperature, in the presence of NO [8], and also by addition of reductants. CO efficiently removes atomic oxygen from the catalyst surface and leads to a substantially decreased operation temperature with respect to the direct N_2O decomposition. The reaction of N_2O with CO is stoichiometric [Eq. (5)] and the N_2O conversion increases linearly with the molar feed CO/N_2O ratio (Fig. 8). The method of preparation and activation of FeMFI zeolites determines the iron constitution, which strongly influences the catalytic performance. Since CO is an efficient oxygen remover, the overall rate of N_2O conversion by SCR can approach that of N_2O activation [Eq. (1)]. This can be used to probe the reactivity of atomic oxygen species (resulting from N_2O activation) adsorbed on the various iron sites identified in Fe-zeolites.

The heterogeneous nature of iron in the samples often complicates interpretations concerning the nature of active species and their relative contribution in the overall reaction. The remarkably uniform distribution of iron in *ex*-Fe-silicalite as isolated Fe ions connected to its high catalytic activity is a strong indication of the importance of mononuclear iron ions in the reduction of N_2O with CO. Fig. 12 shows the derived correlation between the total percentage of isolated Fe sites estimated from the relative intensity of the UV/vis subbands below 280 nm (Table 2) and the catalytic activity for N_2O conversion at 600 K (Fig. 8). The N_2O conversion and the percentage of isolated Fe^{3+} sites between the catalysts (relative to *ex*-Fe-silicalite) are in the same order of magnitude and follow the sequence: Fe/ZSM-5 > *ex*-Fe-silicalite > *ex*-FeZSM-5 ∼ Fe-ZSM-5. The poor catalytic performance of ion-exchanged Fe-ZSM-5 can be expected in view of the extensive iron clustering in the form of large inactive Fe-oxide particles. Iron clustering also occurs in the catalyst prepared by sublimation (Fe/ZSM-5), but the high iron content together with a relatively high fraction of iron in intrazeolitic positions makes it the most active formulation in terms of absolute N_2O conversions. The activity of *ex*-FeZSM-5 is largely reduced compared to *ex*-Fe-silicalite, which correlates with the decreased concentration of isolated iron species due to clustering. However, *ex*-FeZSM-5 was a more effective catalyst than *ex*-Fe-silicalite in direct N_2O decomposition [19,21]. This has been attributed to the intrinsic mechanism of the N_2O conversion investigated, which determines its optimal iron architecture [19,63]. Based on our activity and characterization results with *ex*-Fe-silicalite and the derived correlation in Fig. 12, isolated iron ions are very active toward N_2O activation [Eq. (1)] and the removal of the generated atomic oxygen (O^*) can be efficiently done in the presence of CO. However, in direct N_2O decomposition, the isolated nature of iron in *ex*-Fe-silicalite makes difficult recombination of O^* according to Eq. (3) (rate-determining step), even though the rate of Eq. (1) is higher than over *ex*-FeZSM-5. Finally, it should be noted that the correlation in Fig. 12 assumes that the totality of isolated sites in the steam-activated samples are in extraframework positions. This is the case for *ex*-FeZSM-5, as concluded in [20,21]. For *ex*-Fe-silicalite, even if our characterization and activity data point to an extensive iron extraction, a certain (small) fraction of redox-inactive framework iron cannot be excluded. This fraction was not quantified here, since framework and extraframework species cannot be discriminated in UV/vis spectroscopy. In rigorous terms, the fraction of remaining framework iron in *ex*-Fe-silicalite should be deducted from the total fraction of isolated sites in Fig. 12, since Fe(III) in tetrahedral framework positions do not contribute to the catalytic activity [58].

The above reasoning does not exclude the participation of other iron species in the reaction. In situ spectroscopies

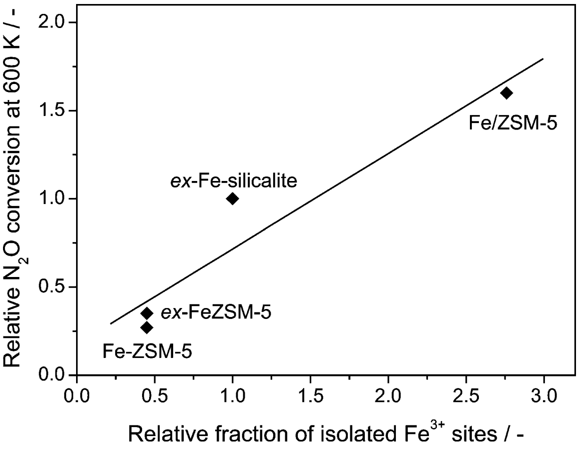

Fig. 12. Correlation between the relative N_2O conversion at 600 K (from Fig. 8) and the relative fraction of isolated Fe^{3+} sites (from Table 2) in the Fe-zeolites investigated. Values are referred to *ex*-Fe-silicalite.

revealed important differences in the redox behavior of the iron species in the catalysts upon interaction with O_2, N_2O, and CO, suggesting that both isolated Fe^{3+} sites as well as oligonuclear $Fe_x^{3+}O_y$ species are active in the reaction of N_2O with CO at 623 K. The reaction mechanism associated to these species differs substantially. In situ UV/vis analyses have clearly shown that Fe(III) in oligonuclear $Fe_x^{3+}O_y$ clusters can be easily reduced by CO to the divalent state and can be completely reoxidized by N_2O (Fig. 9). In combination with EPR results, it can be proposed that the reduction of N_2O with CO over these sites occurs according to Eqs. (7) and (8), i.e., via intermediate formation of O^- radicals. This mechanism agrees with the classical hypothesis stating that CO purely acts as an O scavenger leading to CO_2 [Eq. (7)] and regenerating the active site (□) for subsequent N_2O activation [12–14,19].

$$Fe^{3+}{-}O{-}Fe^{3+} + CO \rightarrow Fe^{2+}{-}\square{-}Fe^{2+} + CO_2, \tag{7}$$

$$Fe^{2+}{-}\square{-}Fe^{2+} + N_2O \rightarrow Fe^{3+}{-}O^{-}{-}Fe^{2+} + N_2. \tag{8}$$

Differently, the (dominant) isolated Fe^{3+} ions in extraframework positions of *ex*-Fe-silicalite suffer no reduction by CO at 623 K (Fig. 9). The relatively weak interaction between CO and iron ions is commonly accepted [43]. However, the changes of the local symmetry and altered position of the signals in the EPR spectra clearly indicate that CO strongly coordinates to ferric ions in *ex*-Fe-silicalite. Attending to these results, the mechanism represented by Eqs. (9) and (10) can be proposed for the N_2O reduction with CO over isolated iron sites.

$$Fe^{3+}{-}\square + CO \rightarrow Fe^{3+}{-}CO, \tag{9}$$

$$Fe^{3+}{-}CO + N_2O \rightarrow Fe^{3+}{-}\square + N_2 + CO_2. \tag{10}$$

This mechanism implies that the involved isolated Fe species must be coordinatively unsaturated in order to chemisorb CO. This holds for species associated with the $g' \sim 2$ as well as the $g' > 5$ signals in *ex*-Fe-silicalite (Fig. 10). The observations related to the latter group of signals are in excellent agreement with various EPR studies, where the reactivity of the EPR signals around $g' \sim 6$ is elaborated. Kucherov et al. [64] determined by in situ EPR that the signals at $g' \sim 5.6$ and 6.5 observed in Fe/ZSM-5 catalysts prepared by sublimation disappear upon contact with NO or NO_2. The corresponding signals were assigned to very reactive coordinatively unsaturated Fe^{3+} species. Volodin et al. [65] also attributed the disappearance of this line (in vacuum and in the presence of water and NO) as an indication for the reactivity of an ion-exchanged FeZSM-5 with N_2O. Ribera et al. [66] found that the signals at $g' \sim 6.4$ and 5.7 in steam-activated FeZSM-5 disappear upon addition of β-mercaptoethanol, concluding their participation in redox processes. In a recent study, Kubánek et al. [67] correlated the intensity of the signals at $g' \sim 6.0$ and 5.6 and the activity of HZSM-5 zeolites with low Fe concentrations in the oxidation of benzene to phenol with N_2O. These signals were assigned to distorted T_d-coordinated isolated ions with a complex oxo structure in cationic sites, as similarly found by us. In our spectra, the signal at $g' \sim 4.3$ shows hardly any changes during treatment with N_2O or CO, and hence is not considered as decisive for the catalytic performance. It can be concluded that the isolated iron ions associated with this signal are not accessible by reactants and/or have no vacant coordination sites.

5. Conclusions

The reduction of N_2O with CO has been investigated over differently prepared Fe-zeolite catalysts. The preparation method determines the nature and distribution of iron species in the final zeolites. Results from the applied techniques to characterize the iron form(s), including HRTEM, UV/vis, and EPR spectroscopy, are in excellent agreement. A common denominator of the Al-containing Fe-zeolites is the heterogeneous constitution with respect to iron and the extensive degree of iron clustering, in the form of oligonuclear iron clusters and large iron oxide particles. Iron association was largely prevented in steam-activated *ex*-Fe-silicalite, which mainly contains isolated iron ions in extraframework positions. CO enhances the N_2O decomposition rate over all the catalysts to lower temperatures with respect to direct N_2O decomposition, and the catalytic activity increases linearly with the molar CO/N_2O feed ratio. The catalytic performance in the N_2O reduction with CO is strongly influenced by the iron constitution in the zeolite. The high specific activity of *ex*-Fe-silicalite, with a remarkable uniform distribution of isolated iron ions, is essential to conclude the importance of mononuclear iron ions in the reduction of N_2O by CO. The highly clustered ion-exchanged FeZSM-5 catalyst shows poor activities in the reaction. Accordingly, a correlation between the N_2O conversion and the fraction of isolated Fe(III) sites in the catalysts has been obtained. In situ UV/vis and EPR studies evidenced the participation of mononuclear iron ions in the N_2O–CO reaction, and also support the involvement of oligonuclear $Fe_x^{3+}O_y$ species. The interaction of N_2O and CO and the reaction mechanism is iron site dependent. Over isolated sites, the reduction of N_2O with CO occurs via coordinated CO species on Fe^{3+} ions, not involving change of oxidation site. The reaction over oligonuclear iron clusters proceeds via a redox Fe^{3+}/Fe^{2+} process via intermediate formation of O^- radicals. These results confirm the relationship between the preferred structure of the active iron site and the associated reaction mechanism and have important implications in oxidation and reduction conversions involving N_2O over Fe-zeolites.

Acknowledgment

Dr. P.J. Kooyman is acknowledged for performing the TEM analysis.

References

[1] F. Kapteijn, J. Rodríguez-Mirasol, J.A. Moulijn, Appl. Catal. B 9 (1996) 25.
[2] J. Pérez-Ramírez, F. Kapteijn, K. Schöffel, J.A. Moulijn, Appl. Catal. B 44 (2003) 117.
[3] G.I. Panov, CATTECH 4 (2000) 18.
[4] C.M. Fu, V.N. Korchak, W.K. Hall, J. Catal. 68 (1981) 166.
[5] J. Leglise, J.O. Petunchi, W.K. Hall, J. Catal. 86 (1984) 392.
[6] J. Pérez-Ramírez, E.V. Kondratenko, Chem. Commun. (2003) 2152.
[7] G. Mul, J. Pérez-Ramírez, F. Kapteijn, J.A. Moulijn, Catal. Lett. 7 (2001) 77.
[8] J. Pérez-Ramírez, F. Kapteijn, G. Mul, J.A. Moulijn, J. Catal. 208 (2002) 211.
[9] T. Nobukawa, S. Tanaka, S. Ito, K. Tomishige, S. Kameoka, K. Kunimori, Catal. Lett. 83 (2002) 5.
[10] R.W. van den Brink, S. Booneveld, J.R. Pels, D.F. Bakker, M.J.F.M. Verhaak, Appl. Catal. B 32 (2001) 73.
[11] G. Delahay, M. Mauvezin, A. Guzmán-Vargas, B. Coq, Catal. Commun. 3 (2002) 385.
[12] F. Kapteijn, G. Mul, G. Marbán, J. Rodríguez-Mirasol, J.A. Moulijn, Stud. Surf. Sci. Catal. 101 (1996) 641.
[13] G.I. Panov, V.I. Sobolev, A.S. Kharitonov, J. Mol. Catal. A: Chem. 61 (1990) 85.
[14] K.A. Dubkov, E.A. Paukshtis, G.I. Panov, Kinet. Catal. 42 (2001) 230.
[15] G. Centi, F. Vazzana, Catal. Today 53 (1999) 683.
[16] R. Joyner, M. Stockenhuber, J. Phys. Chem. B 103 (1999) 5963.
[17] J. Pérez-Ramírez, F. Kapteijn, G. Mul, J.A. Moulijn, Chem. Commun. (2001) 693.
[18] F. Heinrich, C. Schmidt, E. Löffler, M. Menzel, W. Grünert, J. Catal. 212 (2002) 157.
[19] J. Pérez-Ramírez, F. Kapteijn, A. Brückner, J. Catal. 218 (2003) 234.
[20] J. Pérez-Ramírez, G. Mul, F. Kapteijn, J.A. Moulijn, A.R. Overweg, A. Doménech, A. Ribera, I.W.C.E. Arends, J. Catal. 207 (2002) 113.
[21] J. Pérez-Ramírez, F. Kapteijn, J.C. Groen, A. Doménech, G. Mul, J.A. Moulijn, J. Catal. 214 (2003) 33.
[22] H.-Y. Chen, W.M.H. Sachtler, Catal. Today 42 (1998) 73.
[23] A. Brückner, B. Kubias, B. Lücke, Catal. Today 32 (1996) 215.
[24] J. Pérez-Ramírez, R.J. Berger, G. Mul, F. Kapteijn, J.A. Moulijn, Catal. Today 60 (2000) 93.
[25] R.J. Berger, J. Pérez-Ramírez, F. Kapteijn, J.A. Moulijn, Appl. Catal. A 227 (2002) 321.
[26] S. Bordiga, R. Buzzoni, F. Geobaldo, C. Lamberti, E. Giamello, A. Zecchina, G. Leofanti, G. Petrini, G. Tozzolo, G. Vlaic, J. Catal. 158 (1996).
[27] G. Lehmann, Z. Phys. Chem. Neue Folge 72 (1970) 279.
[28] J. Patarin, M.H. Tullier, J. Durr, H. Kessler, Zeolites 12 (1992) 70.
[29] L.E. Iton, R.B. Beal, D.T. Hodul, J. Mol. Catal. A: Chem. 21 (1983) 151.
[30] A. Brückner, R. Lück, W. Wieker, B. Fahlke, H. Mehner, Zeolites 12 (1992) 380.
[31] R. Aasa, J. Chem. Phys. 52 (1983) 3919.
[32] P.N. Joshi, S.V. Awate, V.P. Shiralkar, J. Phys. Chem. 97 (1993) 9749.
[33] T. Inui, H. Nagata, T. Takeguchi, S. Iwamoto, H. Matsuda, M. Inoue, J. Catal. 139 (1993) 482.
[34] A. Brückner, U. Lohse, H. Mehner, Micropor. Mesopor. Mater. 20 (1998) 207.
[35] D. Goldfarb, M. Bernardo, K.G. Strohmaier, D.E.W. Vaughan, H. Thomann, J. Am. Chem. Soc. 116 (1994) 6344.
[36] A.V. Kucherov, A.A. Slinkin, Zeolites 8 (1988) 110.
[37] B. Wichterlová, P. Jiru, React. Kinet. Catal. Lett. 13 (1980) 197.
[38] A.F. Ojo, J. Dwyer, R.V. Parish, Stud. Surf. Sci. Catal. 49 (1989) 227.
[39] P. Wenquin, Q. Shilun, K. Zhiyun, P. Shaoyi, Stud. Surf. Sci. Catal. 49 (1989) 281.
[40] G. Catana, J. Pelgrims, R.A. Schoonheydt, Zeolites 15 (1995) 475.
[41] A. Brückner, in: B.M. Weckhuysen, P. Van Der Voort, G. Catana (Eds.), Spectroscopy of Transition Metal Ions on Surfaces, Leuven Univ. Press, Leuven, 2000, p. 69.
[42] A.V. Kucherov, M. Shelef, J. Catal. 195 (2000) 106.
[43] G. Berlier, G. Spoto, S. Bordiga, G. Ricchiardi, P. Fisicaro, A. Zecchina, I. Rosetti, E. Selli, L. Forni, E. Giamello, C. Lamberti, J. Catal. 208 (2002) 64.
[44] V.A. Shvets, V.B. Kazanski, J. Catal. 25 (1972) 123.
[45] K. Hayashi, M. Hirano, S. Matsuishi, H. Hosono, J. Am. Chem. Soc. 124 (2002) 738.
[46] M. Che, A.J. Tench, Adv. Catal. 31 (1982) 77.
[47] E.V. Starokon, K.A. Dubkov, L.V. Pirutko, G.I. Panov, Top. Catal. 23 (2003) 137.
[48] J. Tang, M. Myers, K.A. Bosnick, L.E. Brus, J. Phys. Chem. B 107 (2003) 7501.
[49] A. Zecchina, S. Bordiga, G. Spoto, A. Damin, G. Berlier, F. Bonino, C. Prestipino, C. Lamberti, Top. Catal. 21 (2002) 67.
[50] P. Marturano, A. Kogelbauer, R. Prins, Stud. Surf. Sci. Catal. 125 (1999) 619.
[51] P. Marturano, L. Drozdová, A. Kogelbauer, R. Prins, J. Catal. 190 (2000) 460.
[52] X. Feng, W.K. Hall, J. Catal. 166 (1997) 368.
[53] W.K. Hall, X. Feng, J. Dumesic, R. Watwe, Catal. Lett. 52 (1998) 13.
[54] P. Marturano, L. Drozdová, A. Kogelbauer, R. Prins, J. Catal. 192 (2000) 236.
[55] A.A. Battiston, J.H. Bitter, F.M.F. de Groot, A.R. Overweg, O. Stephan, J.A. van Bokhoven, P.J. Kooyman, C. van der Spek, G. Vanko, D.C. Koningsberger, J. Catal. 213 (2003) 251.
[56] G. Berlier, A. Zecchina, G. Spoto, G. Ricchiardi, S. Bordiga, C. Lamberti, J. Catal. 215 (2003) 264.
[57] G.I. Panov, A.K. Uriarte, M.A. Rodkin, V.I. Sobolev, Catal. Today 41 (1998) 365.
[58] J. Pérez-Ramírez, F. Kapteijn, G. Mul, J.A. Moulijn, Catal. Commun. 3 (2002) 19.
[59] A.M. Ferreti, C. Oliva, L. Forni, G. Berlier, A. Zecchina, C. Lamberti, J. Catal. 208 (2002) 83.
[60] G. Berlier, G. Spoto, G. Ricchiardi, S. Bordiga, C. Lamberti, A. Zecchina, J. Mol. Catal. A 182–183 (2002) 359.
[61] K.A. Dubkov, N.S. Ovansesyan, A.A. Shteinman, E.V. Starokon, G.I. Panov, J. Catal. 207 (2002) 341.
[62] G. Mul, J. Pérez-Ramírez, F. Kapteijn, J.A. Moulijn, Catal. Lett. 80 (2002) 129.
[63] J. Pérez-Ramírez, A. Brückner, S. Kumar, F. Kapteijn, in: S.D. Jackson, J. Hargreaves, D. Lennon (Eds.), Catalysis in Application, The Royal Society of Chemistry, Cambridge, 2003, p. 308.
[64] A.V. Kucherov, C.N. Montreuil, T.N. Kucherova, M. Shelef, Catal. Lett. 56 (1998) 173.
[65] A.M. Volodin, V.I. Sobolev, G.M. Zhidomirov, Kinet. Catal. 39 (1998) 775.
[66] A. Ribera, I.W.C.E. Arends, S. de Vries, J. Pérez-Ramírez, R.A. Sheldon, J. Catal. 195 (2000) 287.
[67] P. Kubánek, B. Wichterlová, Z. Sobalik, J. Catal. 211 (2002) 109.